*Submitted for Publication in Scripta Materialia in March 2004, Revised in March 2004*

# Compressive Response of A Single Crystalline CoNiAl Shape Memory Alloy

H. E. Karaca[1], I. Karaman[1]*, Y.I. Chumlyakov[2], D.C. Lagoudas[3], and X. Zhang[4]

[1]Department of Mechanical Engineering, Texas A&M University, College Station, TX 77843

[2] Siberian Physical-Technical Institute, Tomsk, 634050, Russia

[3]Department of Aerospace Engineering, Texas A&M University, College Station, TX 77843

[4]Nitinol COE, Edwards LifeSciences, Irvine, CA 92614

*: Corresponding Author: ikaraman@mengr.tamu.edu

## ABSTRACT

The effects of crystallographic orientation and temperature on pseudoelasticity and recoverable strain levels under constant stress are revealed for the Co-31at.%Ni-27at.%Al alloy single crystals under compression. The single crystals demonstrate a perfect pseudoelasticity at temperatures as high as 170 °C, recoverable transformation strains of 4% along the [100] orientation and 2.5% along the [123] orientation, small stress hysteresis (<40MPa) and high strength level against dislocation formation.

**Keywords:** Shape Memory Alloys; CoNiAl; Martensitic Phase Transformation; Pseudoelasticity.

## 1. INTRODUCTION

Ferromagnetic shape memory alloys (FSMAs) have attracted increasing interest since Ullakko *et al*. [1] have observed magnetic field induced strain (MFIS) in NiMnGa alloys. Other FSMAs that have been reported to date are FePd [2], FePt [3], NiFeGa [4], CoNiGa [5-6], CoNiAl [7-9]. The combination of large MFIS coupled with the possibility of rapid response makes FSMAs suitable for a wide range of applications such as actuators and sensors. However, there are certain microstructural and magnetic requirements necessary to obtain large MFIS such as twin boundary mobility, high strength against dislocation formation, low volume change upon transformation, and high magnetic anisotropy energy [9-10]. Although Co-33at.%Ni-29at.%Al polycrystals satisfy the mechanical requirements to obtain MFIS as shown in our previous study [9], a detailed single crystal study is needed to reveal the martensitic transformation characteristics such as the orientation and temperature dependence of transformation strain. This understanding will be beneficial for the future investigations on the magneto-thermo-mechanical

behavior of CoNiAl alloys and to establish a link between single and polycrystalline behavior. CoNiAl alloys have low density, high melting temperature, good corrosion resistance [11] and relatively inexpensive constituents when compared to other FSMAs and NiTi.

In our previous study, the pseudoelastic response and temperature dependence of martensitic transformation were investigated in Co-33at.%Ni-29at.%Al polycrystals under compression. Perfect pseudoelasticity up to 4% with a large pseudoelasticy window (>150 °C) was reported [9] revealing the high strength of the parent phase against defect formation. In the present study, Co-31at.%Ni-27at%Al single crystals along the [100] and [123] orientations are used to investigate the orientation and temperature dependence of pseudoelasticity and recoverable transformation strain levels under compression. The composition of Co-33at.%Ni-29at.%Al was selected to have a martensite start temperature ($M_s$) lower than the room temperature for easy single crystal growth [7]. The [100] orientation is selected since the activation of slip systems in B2 phase is difficult upon loading along this direction because of the {110}<001> and {100}<001> slip systems [12-14]. Since the slip in parent phase would be curtailed, the [100] orientation is expected to result in lower stress and temperature hysteresis as compared to the other directions. The [123] orientation is chosen for comparison purposes. This is the first study reported on the mechanical behavior of CoNiAl single crystals and provides the basic knowledge for understanding the shape memory behavior in CoNiAl alloys.

## II. EXPERIMENTAL PROCEDURE

Co-33 at.% Ni–29 at.% Al alloy has been acquired from Special Metals Corporation, New Hartford, NY. Single crystals were grown using the Bridgman technique in a He atmosphere. Compression samples (4 mm x 4 mm x 8 mm) were cut using electro-discharge machining such that their compression axes are along the [100] or [123] directions. Specimens were homogenized at 1350 °C for 24 hours in sealed quartz tubes filled with argon and quenched in water. The composition of the single crystals was determined to be Co-31.2Ni-27.4 Al (at. %) using inductively coupled plasma-atomic emission spectrometry (ICP-AS). The transmission electron microscopy (TEM) foils were prepared by twin-jet electropolishing with a 20 volume % $H_2SO_4$ in a methanol solution at -15 °C. A JEOL 2010 microscope operated at a nominal accelerating voltage of 200 kV was utilized. The mechanical experiments were conducted using an MTS servohydraulic test frame. A miniature extensometer (3 mm gauge) was used to measure the axial strain. The heating/cooling of the samples was achieved by conduction through

compression plates. The maximum temperature was set at 170 °C due to the operation limit of the extensometer. The temperature variation on the samples during the experiments was ± 2 °C.

### III. EXPERIMENTAL RESULTS

Figures 1.a and b show the bright field TEM image of the present alloy and the corresponding diffraction pattern from two adjacent twins, respectively. The martensite crystal structure is $L1_0$ with an average internal twin thickness of about 100 nm as seen in the figure. The twinning plane is found to be $\{1\bar{1}1\}$ which is the same as that in NiMnGa alloys [15]. The crystals are in single phase without any indication of precipitates. The transformation temperatures are determined to be 70 °C for $M_s$, 47 °C for the martensite finish ($M_f$), 68 °C for the austenite start ($A_s$), and 84 °C for the austenite finish ($A_f$) temperatures using Differential Scanning Calorimetry (DSC) as shown in Figure 1.c. The transformation temperatures are considerably higher than those in polycrystals [9] that can be attributed to the significant change in Ni and Al content during single crystal growth.

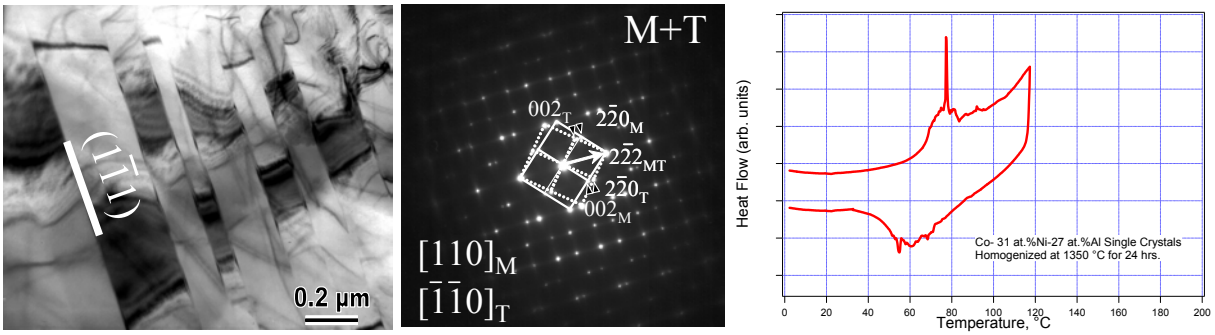


(a) (b) (c)

**Figure 1.** a) Bright field TEM image and b) the corresponding diffraction pattern of the present alloy. (c) DSC response after homogenization and water quenching. The internal twinning plane is determined to be $(1\bar{1}1)$. M: martensite, T: internal twin.

Figure 2 shows the strain vs. temperature response of the [100] and [123] orientations under various values of applied uniaxial compressive stress. The stress is isothermally applied when the material is in austenitic state and then the sample is thermally cycled once between a temperature below $M_f$ and a temperature above $A_f$ under constant uniaxial compressive stress. After one cycle is completed, the stress is increased further in austenite and thermal cycling is repeated. When a non-zero compressive stress is applied, a measurable axial strain is observed as

compared to no observable shape change under zero stress. The possible microstructural mechanism responsible for this behavior is that during cooling under zero stress, a self accommodating structure forms resulting in no net axial strain. Under stress, on the other hand, a favorable martensite variant forms and grows at the expense of other variants and results in a net shape change. Maximum shape memory strains of 4% and 2.5% are obtained for the [100] and [123] orientations, respectively.

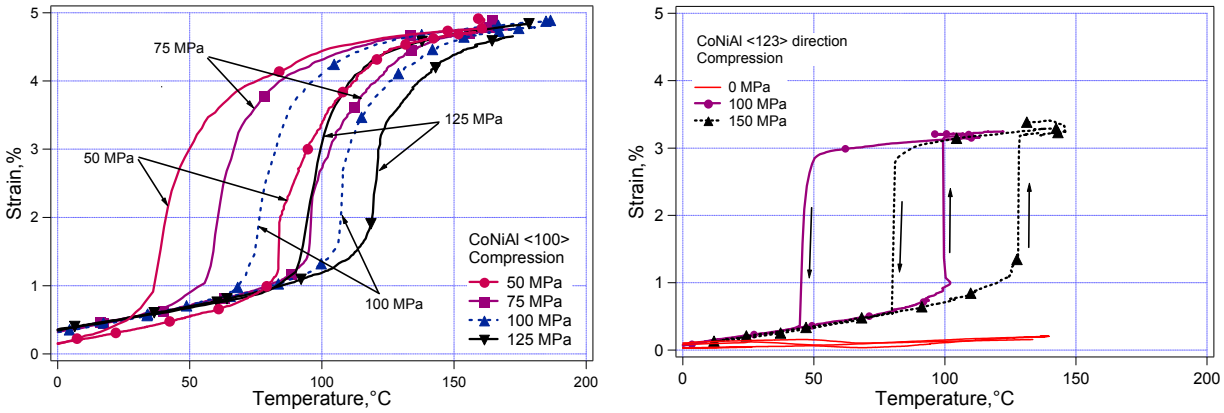


**Figure 2:** Strain vs. temperature response of the a) [100] and b) [123] orientations under constant compressive stress.

In the strain vs. temperature response of the [100] orientation (Figure 2.a), it is difficult to determine the transformation temperatures since the transformation starts and proceeds gradually. To determine the temperature hysteresis as a function of applied stress level, the temperatures at which 50% transformation is completed are used (Figure 3.a). The shape memory strain is measured from the middle of this temperature range and between the extrapolated thermal expansion lines of parent and martensite phases as shown in Figure 3.a and presented in Figure 3.b.

There are three important observations to note in Figures 2 and 3: 1) the orientation dependence of the temperature hysteresis and shape memory strain levels, 2) a decrease in temperature hysteresis as a function of applied stress level and 3) no increase in shape memory strain level as a function of applied stress.

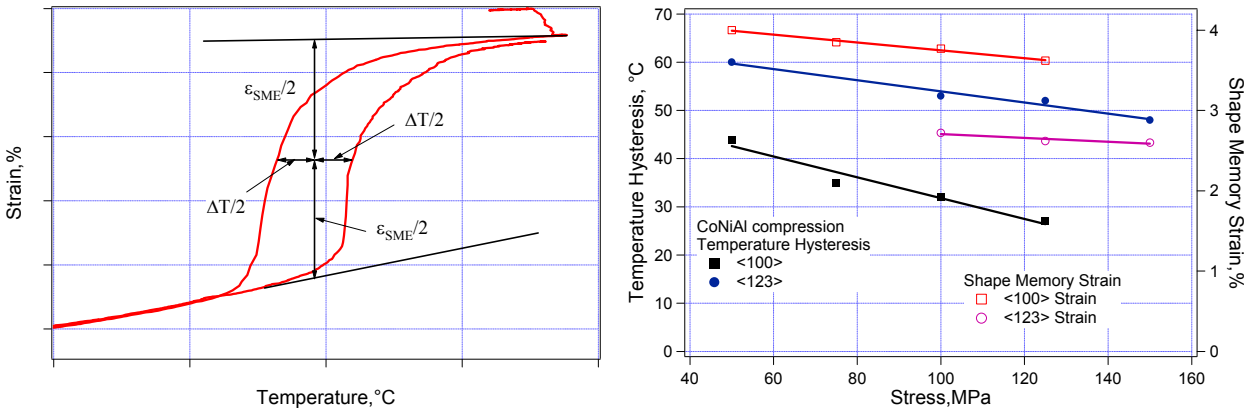


**Figure 3:** a) A schematic for the definitions of the temperature hysteresis (ΔT) and shape memory strain ($\varepsilon_{SME}$), b) Change in ΔT and $\varepsilon_{SME}$ as a function of applied stress along different orientations.

The pseudoelastic response of the [100] orientation at different temperatures is shown in Figure 4.a. Figure 4.b demonstrates the incremental strain response of the same orientation at 170 °C. The notable features are a) a small stress hysteresis (the difference in plateau stress levels during loading and unloading) (~40 MPa); b) a perfect pseudoelastic strain level of 4%; c) a small strain hardening in the plateau region; d) an increase in critical stress for stress induced martensitic transformation (SIM) and elastic modulus with temperature; e) an increase in stress hysteresis with strain level; and f) a high strength for dislocation slip (>1000 MPa).

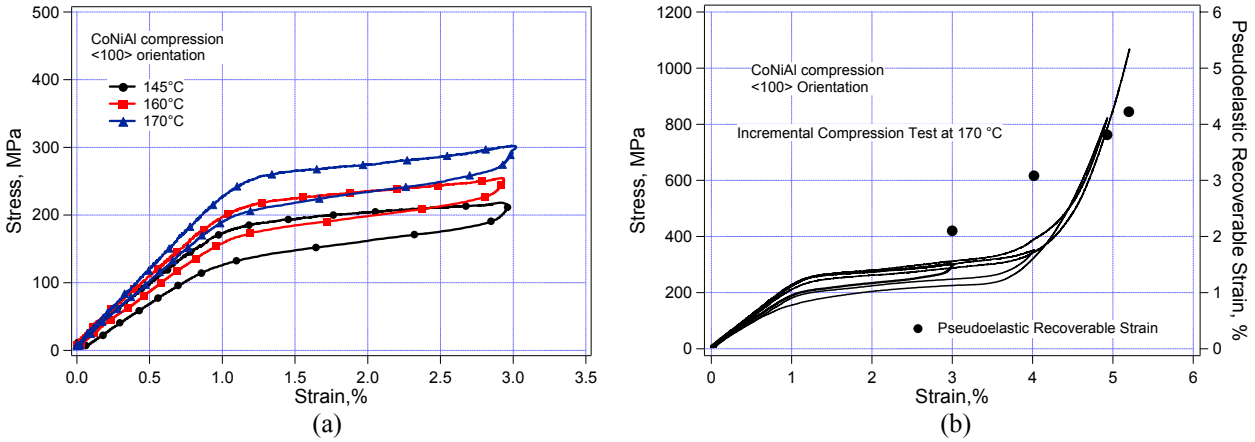


**Figure 4**. a) The temperature and b) strain dependence of the pseudoelastic response of the [100] orientation.

Figure 5 shows the pseudoelastic response of the [123] orientation. The salient differences in the response of the [123] orientation as compared to that of the [100] orientation are: a) strain softening in the plateau region; b) a lower strength for dislocation slip (~900MPa); c) a lower pseudoelastic strain level (2.5 % in the [123] orientation vs. 4% in the [100]

orientation); and (d) higher stress for SIM although the thermal conditions are the same as the [100] orientation.

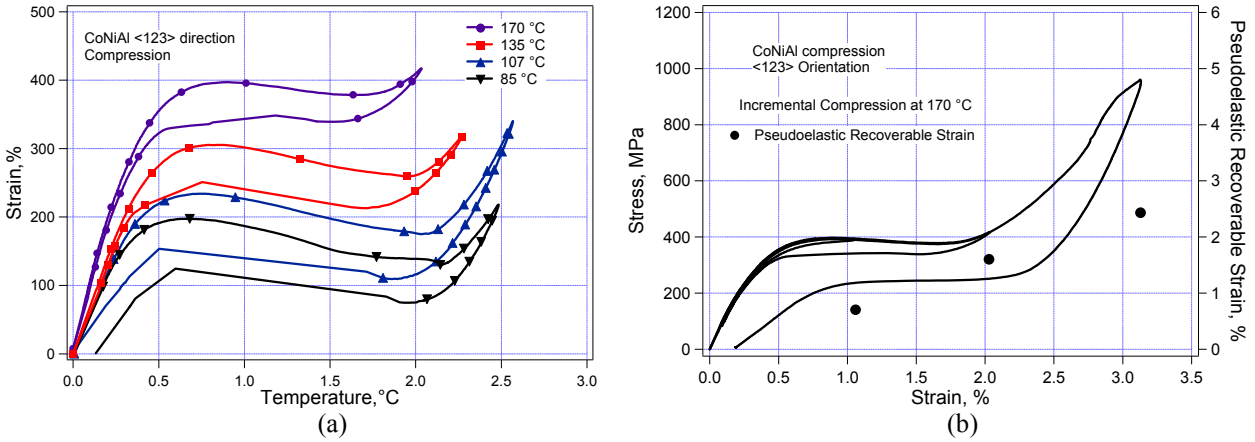


**Figure 5**: a) The temperature and b) the strain dependence of the pseudoelastic response of the [123] orientation.

## IV. DISCUSSION OF THE RESULTS

The origin of the orientation dependence of the shape memory strain presented in Figures 2 and 3.b is mainly the crystallographic relation between the applied stress direction and possible crystallographic systems (transformation shear plane - also known as habit plane - and direction) for parent to martensite transformation. To predict the theoretical transformation strain levels as a function of crystallographic orientation under compression, we use the framework developed based on the "Energy Minimization Theory" [16, 17]. For more detailed description of the theoretical framework, please refer to [18]. Upon B2 to $L1_0$ transformation in CoNiAl, the martensite is composed of internal twins in the $L1_0$ phase as shown in Figure 1. Considering the lattice correspondence between B2 and $L1_0$ phases [19], there are total of 3 variants. In the parent phase coordinate system, the deformation matrices to obtain these variants can be designated as $\boldsymbol{U_1}$, $\boldsymbol{U_2}$ and $\boldsymbol{U_3}$ [17, 18].

For a given variant pair, the twin plane $\boldsymbol{n}$ and twin shear $\boldsymbol{a}$ can be determined provided that the plane is an invariant plane (unrotated and undistorted) [16, 18] using

$$\boldsymbol{R_{ij}U_j - U_i = a \otimes n} \qquad (1)$$

where $\boldsymbol{R_{ij}}$ is an orthogonal tensor and represents the relative rotation between the two variants satisfying $\boldsymbol{R_{ij}^T R_{ij} = I}$ ($\boldsymbol{I}$ is second rank identity tensor and the superscript $T$ represents the transpose of a matrix). The $\otimes$ represents a dyadic product. The twinned martensite is composed

of variant pairs with a certain volume ratio. When there are finite number of twin layers, the deformation of martensite is represented as

$$\boldsymbol{F_M} = \boldsymbol{R_h}\left[f\boldsymbol{R_{ij}}\boldsymbol{U_j} + (1-f)\boldsymbol{U_i}\right] \tag{2}$$

where $\boldsymbol{U_i}$ and $\boldsymbol{U_j}$ are two variants in the twinned martensite and *(1-f)* and *f* are respective volume fractions. The tensor $\boldsymbol{R_h}$ is the relative rotation between the twinned martensite and the parent phase. The habit plane $\boldsymbol{m}$ and transformation shear $\boldsymbol{b}$ can be obtained using

$$\boldsymbol{F_M} - \boldsymbol{I} = \boldsymbol{b} \otimes \boldsymbol{m} \tag{3}$$

where $\boldsymbol{I}$ is the identity tensor representing the undeformed austenite. In these equations, the known parameters are $\boldsymbol{U_i}$, $\boldsymbol{U_j}$, and all the other unknowns can be solved from the equations. The lattice parameters of B2 and $L1_0$ phases must be known. For the B2 phase $a_0 = 0.287\,\text{Å}$, and for the $L1_0$ phase $a = 0.385\,\text{Å}$ and $c = 0.314\,\text{Å}$ [11]. The twin plane obtained from Eq.(1) is $(0\bar{1}1)$, which corresponds to the $(1\bar{1}1)$ plane in martensite basis. The habit plane normal and transformation shear direction are determined to be $\boldsymbol{m}$ = (0.085 0.752 0.654) and $\boldsymbol{b}$ = <0.0670 -0.007 -0.055>. Once the habit plane normal and transformation shear are determined, it is possible to find the transformation strain as

$$\boldsymbol{\varepsilon} = \frac{1}{2}\left(\boldsymbol{F_M^T}.\boldsymbol{F_M} - \boldsymbol{I}\right) = \frac{1}{2}\left[\boldsymbol{b} \otimes \boldsymbol{m} + \boldsymbol{m} \otimes \boldsymbol{b} + (\boldsymbol{b}.\boldsymbol{b})\boldsymbol{m} \otimes \boldsymbol{m}\right] \tag{4}$$

The transformation strain contours are provided in Figure 6.a for compression. As it can be seen in this figure, the transformation strain level is -5.01% for the [100] orientation and -3.07% for the [123] orientation. The experimental measurements of the transformation strain closely matches up with the theoretical calculations showing that the orientation dependence of the transformation strain is purely crystallographic.

The resolved shear stress factor (RSSF) is calculated using

$$\text{RSSF} = (\boldsymbol{b}.\boldsymbol{e})(\boldsymbol{m}.\boldsymbol{e}) / |\boldsymbol{b}| \tag{5}$$

where $\boldsymbol{e}$ denotes the single crystal loading direction and presented in Figure 6.b. RSSF can be used to calculate the stress required for SIM along different orientations if the critical RSS is known. The RSSF is -0.587 for the [100] orientation and -0.328 for the [123] orientation. From these values, one would expect a higher applied stress to start SIM in the [123] orientation than that required in the [100] orientation provided that the materials are in the same thermal condition. That's indeed what is observed at 170 °C as shown in Figures 4 and 5.

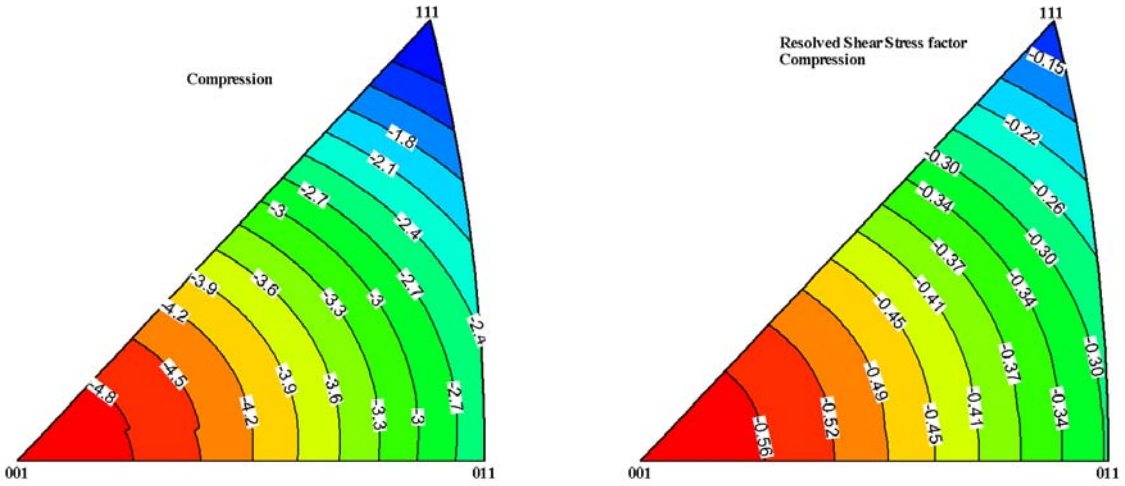


(a) (b)

**Figure 6.** Transformation strain (a) and resolved shear stress factor (b) contours for the B2 to $L1_0$ phase transformation in the present alloy under compression.

The orientation dependence of temperature hysteresis is attributed to the relative difficulty of dislocation slip along certain orientations, in other words, to the difference in the amount of elastic energy relaxed during forward transformation due to the accommodation of martensitic transformation with local dislocation formation. Lower temperature hysteresis in the [100] orientation shows that it is more difficult to activate slip systems in the [100] orientation than the [123] orientation, and thus less elastically stored energy is relaxed. Indeed, in some B2 phase alloys such as NiTi and NiAl, slip systems include {110}<001> and {100}<001> [12-14]. Thus, the [100] orientation is very strong and brittle as slip in B2 phase for axial loading along the [100] orientation is not theoretically possible due to a zero Schmid's factor. It is believed that the same might be true for the B2 phase of the CoNiAl alloy although the slip systems of CoNiAl alloys is not known.

The temperature hysteresis in both orientations decreases with increased applied stress. In conventional SMAs such as CuZnAl and NiTi, the opposite would be expected [18, 20-21]. In NiTi single crystals in solutionized and overaged form, the SME strain and thermal hysteresis increase with applied stress [18, 21]. Large hysteresis in NiTi originates from the partial accommodation of martensitic transformation with dislocations instead of internal twins and

elastic distortion of the matrix [21, 22]. When the stress levels are increased, dislocation formation becomes easier and thermal hysteresis increases.

On the other hand, in peak aged NiTi, the temperature hysteresis decreases with increasing applied stress level similar to the present observation [23, 24**]**. Similarly, the introduction of directional internal stress through marforming or ausforming or mechanical training causes the same decrease in thermal hysteresis [25, 26]. It seems like this effect is encountered when the material strength increases or in other words, the stress required for new dislocation formation, which causes the dissipation of energy, increases. Then, in materials with stronger parent phase, at low stress levels, a mixture of single variant martensite (stress-induced) and self-accommodating variants (thermally induced) form leading to some dissipation by local plasticity due to the variant-variant interaction. When the stress level is increased, the volume fraction of single variant martensite increases leading to less dissipation because of less variant-variant interaction, and thus, lower temperature hysteresis. Moreover, it should be noted that the elastic modulus increases with increasing temperature above $A_f$ as shown in Figure 4. When the stress level is increased, SIM starts at higher temperatures (Figure 2), and thus the amount of elastic energy stored upon martensitic transformation is relatively higher because of the higher elastic modulus. Therefore, the anomalous reduction in thermal hysteresis might also be related to the variation of elastic modulus with temperature.

The lack of increase in SME strain with increasing applied stress level in Figure 3.b is also opposite to what have been observed in NiTi single crystals [21]. In NiTi, higher stress values above a critical level result in local plastic deformation and a decrease in the SME strain and increase in hysteresis. The applied stress of 50 MPa is higher than this critical stress value for CoNiAl since a further increase in applied stress does not result in an increase in SME strain and thermal hysteresis decreases. This can also be linked to the difficulty of dislocation formation in the strong parent phase.

As far as the orientation dependence of the pseudoelastic response is concerned, the observed differences between the [100] and [123] orientations can be attributed to the pure crystallographic effect as described above and more difficult plastic dissipation in the [001] orientation. The stress hysteresis is small as compared to NiTi and CuZnAl alloys. The polycrystalline CoNiAl alloy [9] demonstrated similar small stress hysteresis. The higher strength level against dislocation slip in the [001] orientation can be attributed to the possible slip

systems. The reason for the orientation dependence of the pseudoelastic strain levels is crystallographic similar to the orientation dependence of the SME strain as shown in Figure 6.a. Moreover, these levels are exactly same as the shape memory strain levels which is unusual for common SMAs such as NiTi [27] pointing out again the lack of significant dissipation during SIM.

The stress hysteresis decreases with increasing temperature during isothermal loading as shown in Figure 5.a as opposed to what usually observed in solutionized NiTi [28, 29]. Similar to thermal hysteresis anomaly, significant increase in elastic modulus with increasing temperature and the increase in the volume fraction of single variant martensite due to the increase in the SIM stress level and, thus, less local plastic dissipation, are possible reasons for this decrease. The increase in stress hysteresis with applied strain at a constant temperature (Figures 4.b and 5.b), especially at strain levels in the second "elastic" region, is because of continuing transformation and the formation of more dislocations upon transformation due to higher stress levels in this region. A more pronounced effect is observed in NiTi [30] in this so-called "elastic" region.

From these results we can conclude that the CoNiAl single crystals have high strength against defect formation and a good crystallographic compatibility between the parent and martensite phases where phase and twin boundaries can easily move. This is evident from the low stress and temperature hysteresis and perfect pseudoelasticity. Another unique result of the present study is the observation of perfect pseudoelasticity at temperatures as high as 170 °C.

## V. CONCLUSIONS

Compressive response of a single crystalline Co-31at.%Ni-27at.%Al shape memory alloy was investigated for the first time for pseudoelasticity and shape memory effect. The major findings were:

1) The orientation dependence of shape memory and pesudoelastic strain levels and temperature hysteresis was revealed. Maximum transformation strains in both pseudoelasticity and shape memory experiments were about 4% in the [100] and 2.5% in the [123] orientations under compressive loading which closely matches up with the theoretical calculations based on the "Energy Minimization Theory".

2) The temperature and stress hysteresis decreased with increasing applied stress level and increasing temperature, respectively, which was attributed to the combined effect of high strength matrix and increase in elastic modulus with temperature.
3) The present CoNiAl alloy demonstrated a perfect pseudoelasticty at temperatures as high as 170 °C making CoNiAl alloys a promising candidate for high temperature applications.

**ACKNOWLEDGEMENTS**

This work was supported by Army Research Office, Contract No. DAAD 19-02-1-0261, NSF - Division of Materials Research, Contract No. 0244126, and The U.S. Civilian Research and Development Foundation, Grant No. RE1-2525-TO-03.

**REFERENCES**

1. Ullakko K, Huang JK, Kantner C, Kokorin VV, O'Handley RC. Appl Phys Lett 1996;69:1966.
2. James RD, Wuttig M. Phil Mag A 1998;77:1273.
3. Kakeshita T, Takeuchi T, Fukuda T, Saburi T, Oshima R, Muto S, Kishio K. Mater T JIM 2000;41:882.
4. Oikawa K, Ota T, Ohmori T, Tanaka Y, Morito H, Fujita A, Fujita A, Kainuma R, Fukamichi K, Ishida K. Appl Phys Lett 2002;8:5201.
5. Wuttig M, Li J, Craciunescu C. Scr Mater 2001;44:2393
6. Oikawa K, Ota T, Gejima F, Ohmori T, Kainuma T, Ishida K. Mater Trans 2001;42:2472.
7. Oikawa K, Wulff L, Iijima T, Gejima F, Ohmori T, Fujita A, Fukamichi K, Kainuma R, Ishida K. Appl Phys Lett 2001;79:3290
8. Morito H, Fujita A, Fukamichi A, Kainuma R, Ishida K, Oikawa K. Appl Phys Lett 2002;81:1657
9. Karaca HE, Karaman I, Lagoudas DC, Maier HJ, Chumlyakov YI, Scripta Materialia 2003; 49: 831
10. Kakeshita T, Ullakko K. MRS Bull 2002;27:105
11. Kainuma R, Ise M, Jia CC, Ohtani H, Ishida K. Intermetallics 1996;4:151.
12. Surikova NS, Chumlyakov YI. Fiz Met Metalloved 2000; 89: 98.
13. Hornbogen E, Bruckner G, Gottstein G. Z Metallkd 2002; 93: 3.

14. Miracle DB. Acta Metall Mater 1993; 41:649
15. Pons J, Chernenko VA, Santamarta R, Cesari E. Acta Mater 2000;48:3027.
16. Ball JM, James RD. Arch Rat Mech Anal 1987;100: 13.
17. James RD, Hane KF. Acta Mater 2000;48: 197.
18. Sehitoglu H, Jun J, Zhang X, Karaman I, Chumlyakov Y, Maier HJ, Gall K. Acta Mater 2001; 49: 3609.
19. Chen L, Han Y. Mater Sci Eng 2002; 329-331: 725.
20. Xu H, Tan S, Scripta Metall Mater 1991; 25: 1501.
21. Sehitoglu H, Hamilton R, Canadinc D, Zhang XY, Gall K, Karaman I, Chumlyakov YI, Maier HJ. Metall Mater Trans A 2003; 34: 5
22. Karaman I, Karaca HE, Maier HJ, Luo ZP. Metall Mater Trans A 2003; 34: 2527.
23. Kajiwara S, Kikuchi T, Ogawa K, Matsunaga T, Miyazaki S. Phil Mag Lett 1996; 74: 137.
24. Fukuda T, Deguchi A, Kakeshita T, Saburi T. Mater Trans JIM 1997; 38: 514.
25. Hornbogen E. Acta Mater 1985; 33: 595.
26. Mulder JH, Thoma PE, Beyer J. Mater Charac 1994, 32: 161.
27. Sehitoglu H, Karaman I, Zhang XY, Viswanath A, Chumlyakov YI, Maier HJ. Acta Mater 2001; 49: 3621.
28. Liu YO, Galvin SP. Acta Mater 1997; 45: 4431.
29. Tan SM, Miyazaki S. Mat Sci Eng A 1997; 237: 79.
30. Sehitoglu H, Karaman I, Anderson R, Zhang XY, Gall K, Maier HJ, Chumlyakov YI. Acta Mater 2000; 48: 3311.